

Influence of a helical anisotropy profile on the static and dynamic properties of a soft magnetic layerM. Gloanec,¹ S. Dubourg,¹ O. Acher,² F. Duverger,¹ D. Plessis,¹ and A. Bonneau-Brault¹¹CEA Le Ripault, Laboratoire des Matériaux Optiques et Magnétiques, 37260 Monts, France²HORIBA Jobin Yvon S.A.S., 5 Avenue Arago, 91380 Chilly Mazarin, France

(Received 6 January 2012; revised manuscript received 13 March 2012; published 29 March 2012)

The static and dynamic properties of a soft magnetic layer presenting a helical anisotropy profile have been studied both experimentally and theoretically with the help of one-dimensional (1D) micromagnetic calculations. The aim is to investigate the possibility of achieving an evanescent anisotropy by randomizing the effective anisotropy thanks to a continuous rotation of the samples during a growth process. A general method to evaluate the magnetization dispersion based on the angular measurement of the complex permeability spectra and on the determination of the integral criterion is presented. The maximum randomization of the magnetization in $\text{Co}_{86}\text{Nb}_{10.5}\text{Zr}_{3.5}$ layers is found for the sample rotated 1/2 turn. A significant decrease of the effective anisotropy from 15 to 7 Oe is obtained. The 1D simulations give a good explanation and description of the angular dispersive behavior of the magnetization observed as a function of the rotation speed imposed during growth. However, a discrepancy between measured and calculated resonance frequencies is observed and attributed to short-range fluctuations of the magnetization known as the ripplelike phenomenon. Compared to literature, this effect is particularly strong for a high rotation speed.

DOI: [10.1103/PhysRevB.85.094433](https://doi.org/10.1103/PhysRevB.85.094433)

PACS number(s): 75.78.-n, 75.30.Gw, 75.70.-i

I. INTRODUCTION

Soft ferromagnetic films are used in a variety of high-frequency applications such as magnetic recording media, noise filters, antitheft devices, etc. The potentialities of these materials can be evaluated by the generalized Snoek law and the integral criterion equation. The former provides the trade-off between high permeability levels and high operating frequencies, while the latter establishes that the integral of $\mu'' f df$ is bounded by the square of saturation magnetization multiplied by a constant.¹ This limit has been more recently extended with corrective experimental parameters,² and successfully used as a powerful tool to characterize dynamic magnetic properties.^{3,4}

A challenge for microwave applications is to achieve magnetic materials whose properties can be tuned over a frequency band. One way to accomplish this is to use thin films controlled by a magnetic or electric field. For instance, heterostructures such as laminated insulator and ferromagnetic on the edge (LIFE) under a static field or systems associating magnetostrictive ferromagnetic and piezoelectric layers have been considered.^{5,6} A promising area is to use multifunctional materials as multiferroics which naturally or artificially exhibit both ferroelectricity and ferromagnetism.^{7,8} Other ways involve the development of soft materials that intrinsically possess a high resonance frequency or by imposing on soft materials an elevated effective field thanks to a demagnetizing field or interfacial effects. As an example, the magnitude of the in-plane anisotropy can be tailored during the layer fabrication by inducing high magnetostatic anisotropy thanks to oblique deposition angles.⁹ The effective anisotropy can also be enhanced in multilayered systems such as exchange-coupled spring-magnet structures with soft and hard layers,¹⁰ ferromagnetic/antiferromagnetic systems,¹¹ or soft layers laminated by a nonmagnetic layer $(\text{CoNb/Ta})_n$.¹²

All these magnetic structures have been designed in order to increase the anisotropy, and hence the resonance frequency, with the aim of simultaneously maintaining high levels of

permeability. However, few solutions exist to diminish the anisotropy of soft thin films. To improve the film softness, a rotating field can be applied during annealing.¹³ This thermal treatment leads to a reduced anisotropy as a result of it being randomized. Another approach consists in the juxtaposition of two crossed-anisotropy layers,^{14,15} or in the generation of a domain wall in a sandwiched ferromagnet.¹⁶ These last two attempts have revealed unusual behaviors but no drastic diminution of the operating frequency.

In this work, we investigate the static and dynamic properties of a model system composed of a single soft layer with a helical anisotropy. The helical profile is obtained by imposing a continuous rotation of the samples during the deposition. By increasing the rotation speed, the effective anisotropy might become evanescent.

The literature proposes various methods for characterizing the magnetization distribution due to the anisotropy profile, e.g., vectorial vibrating sample magnetometry (VSM),^{17,18} the transverse biased initial susceptibility technique,¹⁹ and more recently, neutron spin precession,²⁰ or an inductive method with a single-coil device.^{21,22} Here, we present a generalized analysis method based on the angular evaluation of the integral criterion.

II. EXPERIMENTAL SETUP AND THEORETICAL MODEL

Magnetic layers were sputter deposited from a $\text{Co}_{86}\text{Nb}_{10.5}\text{Zr}_{3.5}$ alloy target under an Ar atmosphere (5×10^{-3} mbar) onto 9-mm-diameter glass substrates. The base pressure was lower than 1.5×10^{-6} mbar and the deposition rate was 8 nm/s. The sample holder was mounted on a motorized goniometer, rendering it possible to continuously rotate the sample during sputtering. The thickness of all layers was kept constant at approximately 800 nm. The sample was rotated on a scale from $R = 0$ to 16 turns. An in-plane easy axis was induced by the magnetron field of the cathode. When the growth started, the easy axis induced by the magnetron

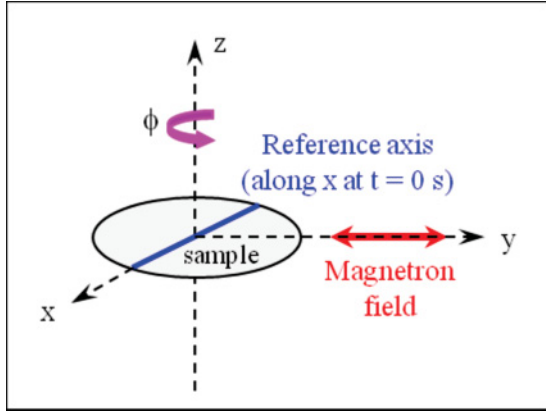


FIG. 1. (Color online) Schematic view of the sample during the growing process.

field was along the y axis, whereas the reference direction is along the x axis, as described in Fig. 1.

The static magnetic properties of the CoNbZr layers were characterized by VSM. The complex permeability spectra were measured from $f = 10$ MHz to 6 GHz by a single-coil perturbation technique.²² For angular measurements, a rotation system displayed in Fig. 2(a) was added to rotate the sample inside the coil. As described in Ref. 23, the calibration procedure involved a prior measurement on the sample saturated with a static magnetic field H_{sat} along the direction of the pumping field h_{RF} . This step made it possible to take dielectric effects into account. Then, to keep the same magnetic history, a saturating static field H_{hist} was applied along the reference direction. The permeability spectra were recorded once the saturating static field was removed. This procedure was repeated for each sample orientation ϕ from the reference direction. It is illustrated in Fig. 2(b).

Recently, Dubuget *et al.* have proposed a method to quantify the anisotropy axis distribution from the angular measurement of the initial permeability assuming a known distribution law.²¹ Here, the analysis is based on the whole permeability spectrum and no particular distribution law is required. By considering the polar coordinate system, the matter fraction with a magnetization orientation between θ and $\theta + d\theta$ could

be represented by the quantity $m(\theta)d\theta$ with $m(\theta) = m(\theta + 2\pi)$. Since $m(\theta)$ is a 2π -periodic function we assume that it could be decomposed into Fourier series

$$m(\theta) = 1/\pi \left[1/2 + \sum_{n=1}^{\infty} a_n \cos(n\theta) + b_n \sin(n\theta) \right], \quad (1)$$

where $a_n = \int_0^{2\pi} m(\theta) \cos(n\theta) d\theta$ and $b_n = \int_0^{2\pi} m(\theta) \sin(n\theta) d\theta$.

The integral of $m(\theta)$ between 0 and 2π is unity. Let us define the permeability of the fraction $m(\theta)d\theta$ along its hard axis $\mu_h(\theta, f)$. The complex permeability of the whole sample measured along the direction ϕ can be written as

$$\mu(\phi, f) \approx \int_0^{2\pi} m(\theta) \mu_h(\theta, f) \sin^2(\phi - \theta) d\theta. \quad (2)$$

Case 1. $\mu_h(\theta, f)$ is independent of θ . In other words, the effective field that contains the terms of exchange, anisotropy, and demagnetizing field, is constant over the sample thickness.

Equation (2) can be written as

$$\begin{aligned} \mu(\phi, f) &\approx \mu_h(f) \left[1 - \cos(2\phi) \int_0^{2\pi} m(\theta) \cos(2\theta) d\theta \right. \\ &\quad \left. - \sin(2\phi) \int_0^{2\pi} m(\theta) \sin(2\theta) d\theta \right] / 2 \\ &\approx \mu_h(f) [1 - a_2 \cos(2\phi) - b_2 \sin(2\phi)] / 2. \end{aligned} \quad (3)$$

Note that Eq. (3) remains valid with a dispersed effective field intensity as long as this dispersion is the same for each angle θ . At each frequency, the angular variation of the permeability $\mu(\phi)$ is a function of three parameters μ_h , a_2 , and b_2 which can be easily obtained by considering three measurement directions $\phi = 0^\circ, 45^\circ, \text{ and } 90^\circ$:

$$\begin{aligned} \mu_h &= \mu(0^\circ) + \mu(90^\circ), \quad a_2 = [1 - 2\mu(0^\circ/\mu_h)], \\ b_2 &= [1 - 2\mu(45^\circ/\mu_h)]. \end{aligned} \quad (4)$$

Let us assume that the quantity $D = (a_2^2 + b_2^2)^{1/2}$ is a magnetization dispersion criterion. In the case of a pure uniaxial system, $m(\theta)$ is characterized by a Dirac function and the quantity D equals unity. On the other hand, in the case of an isotropic system, $m(\theta)$ is a constant and the dispersion

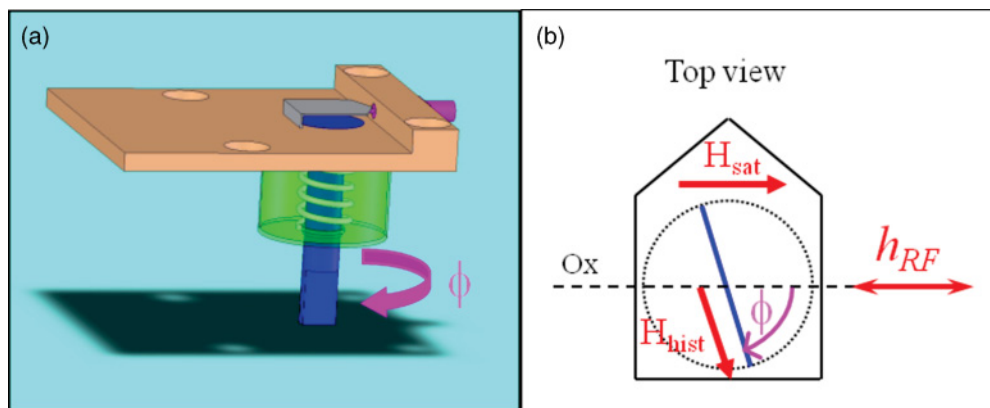


FIG. 2. (Color online) (a) Measurement setup. (b) Top view. At $\phi = 0^\circ$, the reference direction (blue line) was aligned with the dynamic field h_{RF} .

criterion D is null. A similar approach has been successfully employed in the case of a low randomly dispersed sample assuming a periodic Bessel-like $m(\theta)$ function.²¹ This method is adapted to thin films presenting a low angular dispersion and for which the exchange interaction can be neglected. It renders it possible to determine the anisotropy axis dispersion induced by the deposition process.

Case 2. General case $\mu_h(\theta, f)$ depends on θ .

Let us assume that $\mu_h(\theta, f)$ can be expressed as a linear combination of the Bloch-Bloemberger permeability expression. The principle of causality applied to $\mu_h(\theta, f)$ shows that^{1,2,4}

$$\int_0^\infty \mu_h''(\theta, f) f df \approx \pi/2 (\gamma 4\pi M_S)^2. \quad (5)$$

When the upper integral boundary F is large enough compared to the upper resonance frequency $f_{\text{res}}^{\text{max}}$ associated to the longer effective field $H_{\text{eff}}^{\text{max}}$ used in the $\mu_h(\theta, f)$ expression, we obtain

$$\begin{aligned} \int_0^F \mu_h''(\theta, f) f df &\approx \pi/2 (\gamma 4\pi M_S)^2 [1 - t - s] \\ &\approx \pi/2 (\gamma 4\pi M_S)^2, \end{aligned} \quad (6)$$

where $\gamma = \gamma/2\pi$, M_S is the saturation magnetization, and s and t are corrective terms associated to the skin effect and finite truncation.² Let us calculate the microwave permeability integral on the whole sample permeability measured in the

angle ϕ :

$$\begin{aligned} I(\phi) &= \int_0^F \mu''(\phi, f) f df \\ &\approx \int_0^{2\pi} m(\theta) \int_0^F \mu_h''(\theta, f) f df \sin^2(\phi - \theta) d\theta \\ &\approx \pi/2 (\gamma 4\pi M_S)^2 \int_0^{2\pi} m(\theta) \sin^2(\phi - \theta) d\theta \\ &\approx I_{\text{max}} [1 - a_2 \cos(2\phi) - b_2 \sin(2\phi)]/2, \end{aligned} \quad (7)$$

where I_{max} , a_2 , b_2 , and the dispersion criterion D are experimentally obtained with

$$\begin{aligned} I_{\text{max}} &= I(0^\circ) + I(90^\circ), \quad a_2 = [1 - 2I(0^\circ)/I_{\text{max}}], \\ b_2 &= [1 - 2I(45^\circ)/I_{\text{max}}], \quad \text{and} \quad D = (a_2^2 + b_2^2)^{1/2}. \end{aligned} \quad (8)$$

This method is based on the angular evaluation of the integral criterion and allows us to quantify the magnetization dispersion without assuming any particular magnetization distribution law. It is a more general way to calculate the D coefficient deduced in case 1.

III. RESULTS

Figure 3 displays the easy and hard axis hysteresis loops measured on the samples grown with a continuous rotation R of 0, 1/6, 1/2, and 16 turns. For $R = 0$, the easy axis hysteresis loop is typical of soft materials with a square shape and a very low coercivity (<1 Oe). When the field is applied along the

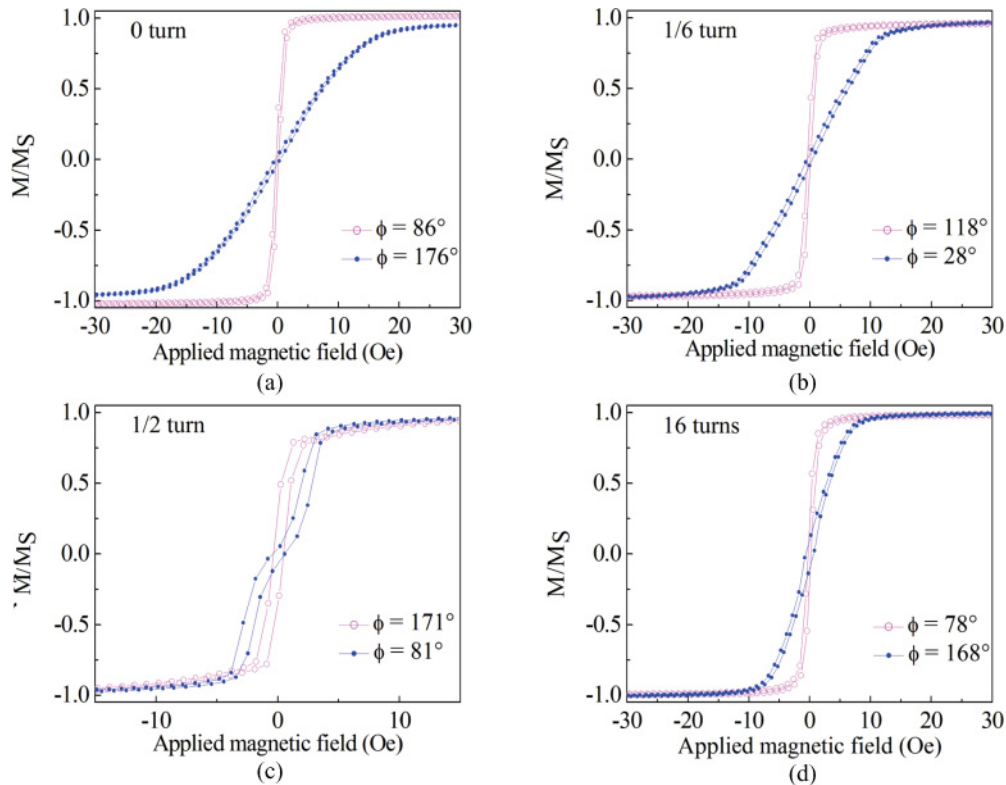


FIG. 3. (Color online) Easy and hard axis hysteresis loops measured on the samples sputtered with a continuous rotation of (a) 0 turn, (b) 1/6 turn, (c) 1/2 turn, and (d) 16 turns. For each sample, the easy (hard) axis direction was deduced from the minimum (maximum) value of the angular variation of the $I(\phi)/I_{\text{max}}$ curve measured by the single-coil technique as described in Fig. 5.

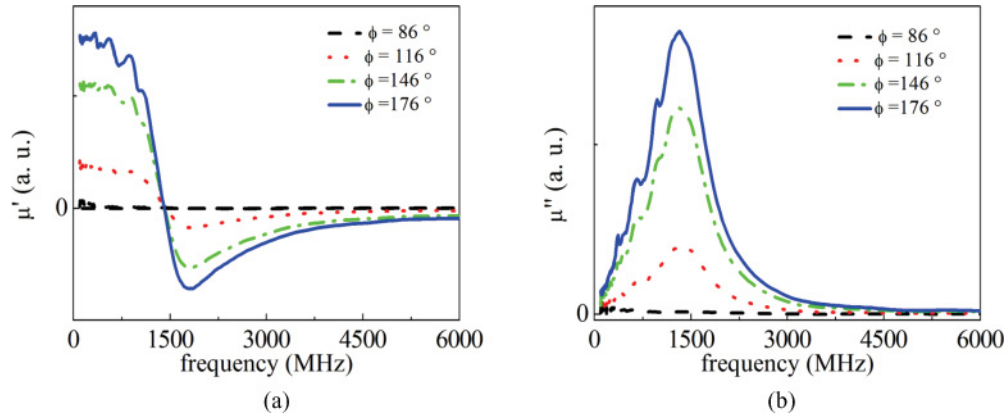


FIG. 4. (Color online) (a) Real and (b) imaginary parts of the permeability spectra measured for the 0-turn sample along different orientations ϕ with respect to the reference direction.

effective hard axis, the magnetization curve becomes slanted and reversible. The anisotropy field $H_K = 15$ Oe deduced from the slope is in agreement with those typically observed in literature.³⁴ Up to a rotation of 1/6 turn, H_K diminishes down to 12 Oe as expected. For 1/2 turn, the hard axis loop plotted in Fig. 3(c) presents a double slope. The same static magnetic behavior is observed for the sample sputtered with $R = 1/3$ (not shown). This unusual hysteresis shape has already been observed and explained in crossed-anisotropy bilayers such as NiFe/NiFe and YCo₂/YCo₂ and in CoNbZr layers annealed under an applied field.^{24,25} It was attributed to competing uniaxial and biaxial anisotropies that resulted from the coupled individual anisotropy axes. For a rotation of 1 turn and more, the hysteresis loops are more typical of easy and hard axes. The anisotropy field H_K remains constant at 7 Oe. It should be noted that an enlargement of the hard axis loop occurs at the field values close to $H = 0$ for high rotation as described in Fig. 3(d).

Figure 4 shows the complex permeability spectra of the 0-turn sample at different orientations ϕ with respect to the reference direction. For $\phi = 86^\circ$, no signal is observed since the pumping field h_{RF} is applied along a well-defined easy axis. On the other hand, the levels of permeability, μ' and μ'' , reach a maximum value at $\phi = 176^\circ$ when h_{RF} becomes normal to the magnetization direction. The small oscillations that can be seen on the spectra at low frequencies are associated with domain-wall vibration modes.²⁶

Figure 5 displays examples of the experimental integral $I(\phi)/I_{max}$ deduced from the complex permeability spectra by following the method described in Sec. II. For the 0-turn sample, the maximal amplitude of the experimental $I(\phi)/I_{max}$ curve and the minimum close to 0 observed at $\phi = 86^\circ$ correspond to the well-defined anisotropy axis along this angular position. When a sample rotation is introduced during sputtering, a drastic decrease of the amplitude occurs, indicating that the magnetization is distributed. This is clearly observable for the 1/2-turn sample with a ratio $I(\phi)/I_{max}$ varying between 0.33 and 0.63. The rotation during the deposition can also involve a shift of the easy direction as illustrated by the 1/6- and 1/2-turn samples for which the easiest axes are measured at $\phi = 110^\circ$ and $\phi = 171^\circ$,

respectively. These values correspond to shifts close to 30° and 90° from the reference direction in agreement with those expected for a helical anisotropy on an angular range of 60° and 180° , respectively. For the high-speed rotation samples, such as the 8-turn one, the amplitude of the $I(\phi)/I_{max}$ curves increases again to reach a value close to the 0-turn sample. This result indicates that the magnetization no longer follows the anisotropy axes induced during the deposition when the anisotropy presents a high number of turns. In other words, the magnetization is no longer angularly distributed at elevated rotation speeds.

The experimental dispersion criteria D and the easiest axis orientation ϕ_{EA} as a function of the turn number R are displayed in Fig. 6. Increasing the rotation to 1/2 during the sample deposition leads to a drop in quantity D from unity (associated to a uniaxial system) to 0.29. When increasing the rotation speed even further, the dispersion criterion tends toward the value of 0.9 with slight variations between 0.8 and 1. In other words, the maximal randomization of the magnetization is obtained for the 1/2-turn sample. Beyond this, the magnetization has a tendency to line up along a direction that minimizes the magnetic energy of the system and corresponds to the easiest axis. As illustrated in Fig. 6(b), the values of the latter show oscillations as a function of the turn fraction.

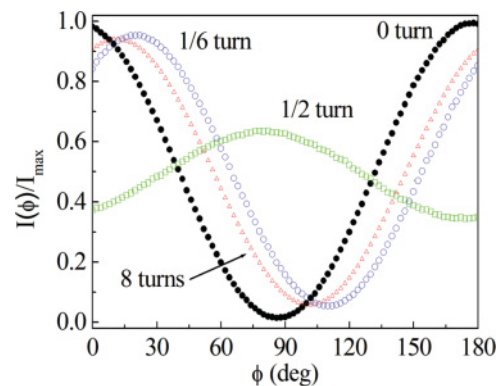


FIG. 5. (Color online) Angular variations of the experimental integral $I(\phi)/I_{max}$ obtained for the 0-, 1/6-, 1/2-, and 8-turn systems.

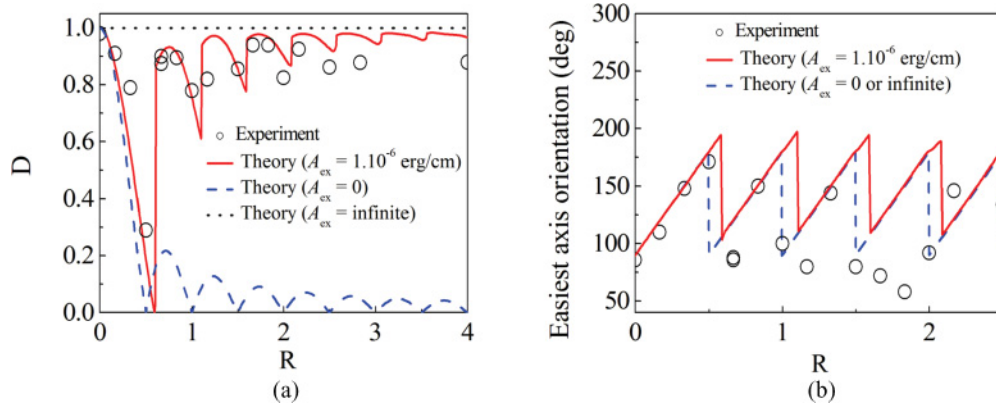


FIG. 6. (Color online) (a) Experimental (open circles) and theoretical (line) dispersion criterion D as a function of the turn number R . (b) Corresponding experimental (open circles) and theoretical (line) easiest axis orientation ϕ_{EA} . The analytical cases of $A_{\text{ex}} = 0$ and infinite A_{ex} are reported too.

The experimental data have been compared to static one-dimensional (1D) micromagnetic simulations. The 1D model assumes an anisotropy with a helical orientation into the layer thickness, i.e., the orientation θ_K of the anisotropy axis varies linearly as a function of the position z into the layer thickness, while the anisotropy constant $K(z)$ remains unchanged. Following Ref. 15, the total micromagnetic energy density can be written as

$$E = \frac{1}{t} \int_0^t \left\{ A_{\text{ex}} \left(\frac{d\theta}{dz} \right)^2 + K \sin^2 [\theta(z) - \theta_K(z)] \right\} dz, \quad (9)$$

where A_{ex} is the exchange constant, θ is the magnetization orientation, and t is the thickness of the layer. Magnetization profiles $\theta(z)$ and corresponding linear anisotropy profiles $\theta_K(z)$ calculated for $R = 1/6, 1/2, 1$, and 16 turns are plotted in Fig. 7. The parameters used for the simulations are a saturation magnetization $M_S = 900$ emu/cm³ and an exchange constant $A_{\text{ex}} = 1.10^{-6}$ erg/cm as expected for CoNbZr with a high Co content,²⁷ an anisotropy field $H_{K0} = 2K/M_S = 15$ Oe as found in magnetometry for the 0-turn sample, and a thickness $t = 800$ nm. In addition, we assume $d\theta/dz = 0$ on the edges of the layer.

Two types of behavior are observed. While the rotation increases from 0 to 0.6 turn, the magnetization orientation follows the $\theta_K(z)$ curve except at the edges of the layer due to the free surface assumption in the calculations [Figs. 7(a) and 7(b)]. This divergence increases with the rotation because of the exchange that tends to align the magnetic moments. Beyond this rotation $R = 0.6$, such as for the 1-turn sample in Fig. 7(c), the magnetization no longer follows the anisotropy profile but oscillates weakly around the easiest axis direction. The angular amplitude of these oscillations decreases as R is raised, whereas their frequency increases in the thickness of the layer. Finally, for the high rotations such as for the 16-turn sample in Fig. 7(d), the magnetization is uniform along the direction given by ϕ_{EA} . These two tendencies depict the two cases of “thick films” and “thin films” in comparison with a Bloch wall width evaluated to $\pi(A_{\text{ex}}/K)^{1/2} \cong 380$ nm.

From the calculations of the static magnetization profiles, we could simulate the complex permeability spectra with a

gyromagnetic ratio $\gamma = 3$ MHz Oe⁻¹, a damping parameter $\alpha = 0.015$, and, taking the skin effect into account, a typical value of resistivity for amorphous CoNbZr $\rho = 140 \times 10^{-8}$ Ω m. Then, the theoretical dispersion criterion D and the easiest axis orientation ϕ_{EA} were deduced according to the method presented in the experimental part. The simulations of D and ϕ_{EA} with $A_{\text{ex}} = 1.0 \times 10^{-6}$ erg/cm displayed in Fig. 6 give a good description of the experimental data. In particular, the dramatic drop of D , the continuous increase of ϕ_{EA} for low R values, and the oscillations of D beyond 1/2 turn are well reproduced by the calculations. To gain more insight into the behavior of the magnetization, let us consider first the analytical cases of infinite A_{ex} and $A_{\text{ex}} = 0$ reported in Fig. 6. In the former case, the magnetization is uniform so that D is unity and the energy density of the system is written as

$$\begin{aligned} E &= \int_{\pi/2}^{\pi/2+2\pi R} \left[\frac{K}{2\pi R} \sin^2(\theta - \theta_K) \right] d\theta_K \\ &= K \frac{\sin(2\pi R)}{2\pi R} \cos^2(\theta - \pi R). \end{aligned} \quad (10)$$

The total anisotropy energy density expression is similar to the one of a uniform uniaxial sample with a fluctuating anisotropy constant equal to $K|\sin(2\pi R)/(2\pi R)$ and an easiest axis orientation that jumps every 1/2 turn, as illustrated in Fig. 6. For the $A_{\text{ex}} = 0$ case, the magnetization orientation $\theta(z)$ follows perfectly the anisotropy direction $\theta_K(z)$. By considering Eqs. (1) and (8) and by defining the truncation function $\text{trunc}(R)$ as the integer part of the turn number R , we can easily deduce

$$\begin{aligned} a_2 &= \frac{1}{4\pi R} \sin \{4\pi [R - \text{trunc}(R)]\}, \\ b_2 &= \frac{1}{4\pi R} (1 - \cos \{4\pi [R - \text{trunc}(R)]\}), \quad \text{and} \quad (11) \\ D &= \frac{|\sin(2\pi R)|}{2\pi R}. \end{aligned}$$

Introducing exchange leads to delay of the first jump of the easiest axis orientation. Indeed, as illustrated in Fig. 6,

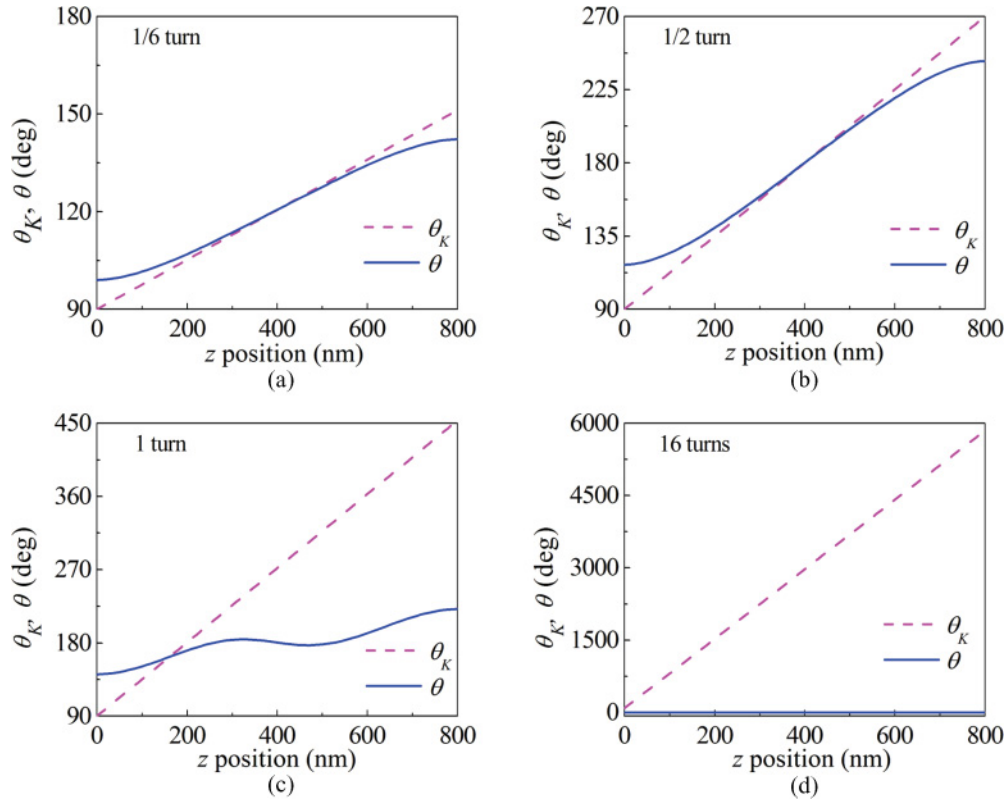


FIG. 7. (Color online) Magnetization profiles $\theta(z)$ and the corresponding linear anisotropy profiles $\theta_K(z)$ calculated for (a) 1/6 turn, (b) 1/2 turn, (c) 1 turn, and (d) 16 turns.

the maximal randomization of the magnetization and the first jump of ϕ_{EA} appears for the 0.6 turn instead of 0.5 with $A_{ex} = 1.0 \times 10^{-6}$ erg/cm. In addition, compared to the case of fully decoupled magnetic moments, the values of D tend to unity when the rotation speed is raised. This is due to the thickness of the layer, which allows here only one complete rotation of the magnetization. Consequently, the behavior observed for high R approaches the one of the infinite A_{ex} case for which D is unity.

Figure 8 shows a comparison between the resonance frequencies measured and calculated for a pumping field normal to the easiest axis. Let us consider again the two analytical cases. With no exchange, the resonance frequency is expected to be constant as a function of the rotation speed since the magnetic moments are independent and to be equal to $\gamma(4\pi M_S H_{K0})^{1/2}$. For the infinite A_{ex} case, the variation of f_{res} is given by $\gamma[4\pi M_S H_{K0} |\sin(2\pi R)| / (2\pi R)]^{1/2}$ as deduced from Eq. (10) and show oscillations. The variation of f_{res} calculated with $A_{ex} = 1.0 \times 10^{-6}$ erg/cm tends to follow the first analytical case for $R < 0.6$ turn and the infinite one for $R > 0.6$ turn. In other words, as shown in the last paragraph, the behavior of the magnetization approaches the one of the fully uncoupled magnetic moments for low R values and tends to the infinite case for high R value ($R < 0.6$). The tendency for the experimental resonance frequencies displayed in Fig. 8(a) is a decrease as R is raised with $f_{res} = 1410$ MHz for the 0-turn case and $f_{res} = 970$ MHz for the 16-turn sample. This reduction due to the anisotropy randomization is far weaker than the drastic drop predicted by the calculations. However,

both the experimental and calculated resonance frequencies show oscillations.

We note that the experimental f_{res} exceeds the value expected with the magnetic anisotropy field H_K measured by magnetometry. This result is illustrated in Fig. 8(a) for the 0-turn and 16-turn samples (large open circles) for which the f_{res} shift is 175 and 190 MHz, respectively. In order to obtain more insight into this disagreement, we realized transverse biased permeability measurements with the magnetic field applied along and perpendicular to the easy axis. The resonance frequencies picked up on the permeability spectra of the 0-turn and 16-turn samples are plotted in Fig. 9. For both samples we observe that the crossing of the linear extrapolations of $f_{res}^2(H)$ with the magnetic field axis provides H_K values that differ depending on the applied field direction. For the sample without a rotation treatment, the H_K values are 17 and 11 Oe, while in the case of 16 turns the corresponding results are 10 and 2 Oe. It should be highlighted that the amplitude of the asymmetry for the 16-turn sample is particularly strong compared to others reported in literature.^{28,29} This asymmetry is generally attributed to magnetization ripple. According to the ripple theory of Hoffmann, f_{res}^2 can be written as^{30,31}

$$f_{res}^2 = \gamma^2 4\pi M_S H_K [(H/H_K \pm 1) + b(H/H_K \pm 1)^{-1/4} + c(H/H_K \pm 1)^{-1}], \quad (12)$$

where the plus sign (minus sign) is used for a static magnetic field applied along (normal to) the easy direction. Moreover, b and c designate the phenomenological parameters describing

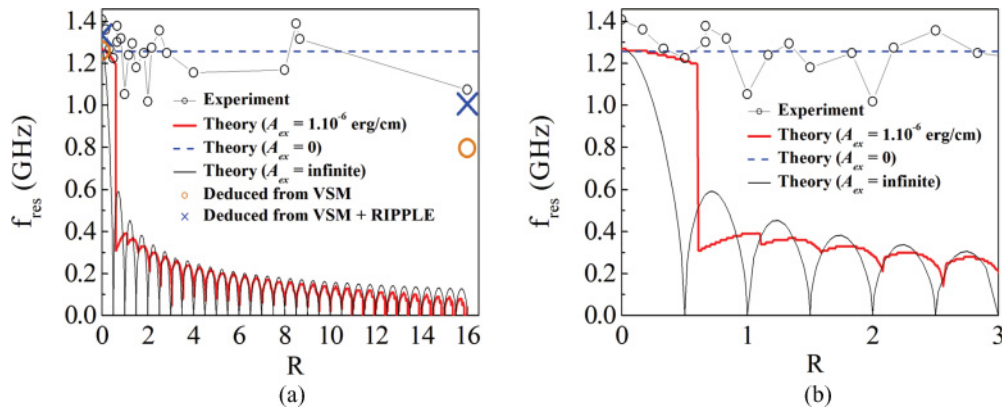


FIG. 8. (Color online) (a) Experimental and calculated resonance frequencies observed for a pumping field normal to the easiest axis. (b) Zoom on the scale from $R = 0$ to 3 turns. The oscillations are observed on both experimental and theoretical f_{res} .

the short-range fluctuations of the magnetization (ripple) and the long-range fluctuations of the magnetic anisotropy (skew), respectively. This last term is found to be negligible in our samples as it has been reported for amorphous CoZrTb thin films or in CoZrNd layers.^{29,32} The best fits of the $f_{res}^2(H)$ curves in the region $H > H_K$ have been obtained by using the anisotropy field parameters $H_K(0 \text{ turn}) = 14.8 \text{ Oe}$, $H_K(16 \text{ turns}) = 6.8 \text{ Oe}$ and $b(0 \text{ turn}) = 0.26$, $b(16 \text{ turns}) = 0.93$. First, we note that the anisotropy field parameters are in very good agreement with the values of 15 and 7 Oe measured by magnetometry for the 0-turn and 16-turn samples, respectively. Secondly, while 0.26 is a typical value for CoNbZr, 0.93 is quite high in comparison with the values generally found in literature.^{28,31} The rotation speed induces the magnetization ripplelike phenomenon which is translated in a microwave regime by a positive shift of the resonance frequency in a zero static magnetic field. Hence, this phenomenon explains the apparent discrepancy between the anisotropy values obtained by VSM and the single-coil technique and, consequently, part of the disagreement between the measured and calculated resonance frequencies.

We underline that the sample studied here is weakly magnetostrictive,³³ presents properties typical of soft amorphous materials, and has a well-defined easy axis in the 0-turn case. Hence, we believe the results presented in this

paper are representative of soft amorphous materials. Now, the reasons for which the effective anisotropy cannot definitively vanish, or, in other words, why a discrepancy between the f_{res} values measured and predicted by the 1D simulations still exist once the ripplelike phenomenon contribution is removed, are unclear. We can postulate several possible effects. First, we can take into account the influence of the adjacent layers on the anisotropy. Indeed, the Suits study led on a crossed-anisotropy bilayer has revealed that during the deposition the top layer anisotropy can impose the anisotropy orientation of the identical-thickness bottom layer.¹⁴ Considering the good description of the magnetization dispersion criterion behavior by the 1D model, this influence is slight in the system studied. Secondly, we must note that the sample should present a magnetic domain structure which is not taken into account in the 1D simulation. Finally, we might consider the magnetostrictive effects which could generate a dispersion of the anisotropy intensity. The deposition procedure used in this study and implying sample rotations could be at the origin of elevated stress and constraints in the thickness of the layer. But, this effect is expected to be quite weak because of the well-known low magnetostriction of the $\text{Co}_{86}\text{Nb}_{10.5}\text{Zr}_{3.5}$ composition used. Consequently, we cannot exclude more fundamental reasons to explain why the evanescent anisotropy cannot be achieved.

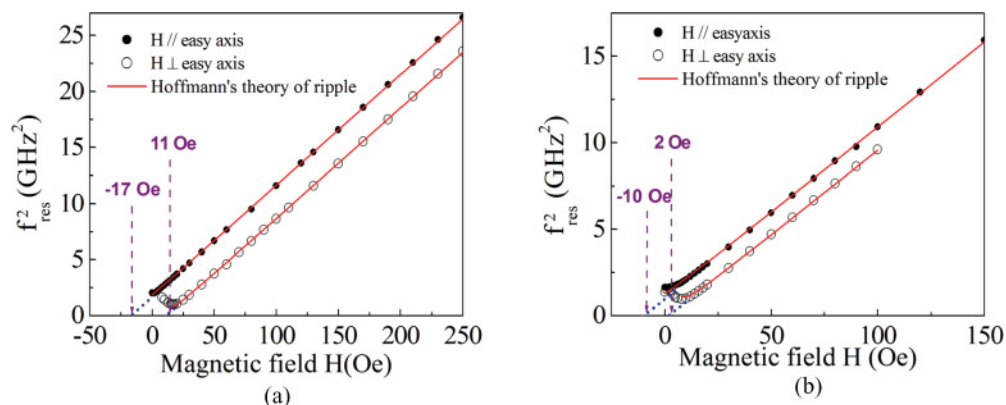


FIG. 9. (Color online) f_{res}^2 curves as a function of the static magnetic field applied for the (a) 0-turn and (b) 16-turn samples.

IV. SUMMARY

The present article has proposed a general method to evaluate the magnetization dispersion. This method is based on the integral criterion measurement and has been successfully applied on a CoNbZr soft magnetic layer with a helical anisotropy profile. The 1D micromagnetic calculation taking into account both the exchange and the helical anisotropy profile provides a good description of the variations of the D dispersion criteria and the easiest axis orientation. The continuous rotation of the samples during sputtering gives rise to a significant drop of the anisotropy field H_K by the randomization of the anisotropy;

however, no evanescent anisotropy has been observed. A discrepancy between resonance frequency measured by the single-coil perturbation technique and VSM is observed and attributed to the short-range fluctuations of the magnetization. This ripplelike phenomenon is found to be very strong for high rotation speeds during the layer deposition.

ACKNOWLEDGMENT

The authors would like to thank A. Thiaville for fruitful discussions.

-
- ¹O. Acher and A. L. Adenot, *Phys. Rev. B* **62**, 11324 (2000).
²O. Acher and S. Dubourg, *Phys. Rev. B* **77**, 104440 (2008).
³L. T. Hung, N. N. Phuoc, and C. K. Ong, *J. Appl. Phys.* **106**, 063907 (2009).
⁴A. Bonneau-Brault, S. Dubourg, V. Dubuget, D. Plessis, and F. Duverger, *J. Phys.: Conf. Ser.* **303**, 012088 (2011).
⁵E. Salahun, G. Tanné, P. Quéffélec, M. Lefloch, A.-L. Adenot, and O. Acher, *Microwave Opt. Technol. Lett.* **30**, 272 (2001).
⁶S. De Blasi, P. Quéffélec, S. Dubourg, O. Bodin, and M. Ledieu, *IEEE Trans. Magn.* **43**, 2651 (2007).
⁷D. O'Flynn, C. V. Tomy, M. R. Lees, A. Daoud-Aladine, and G. Balakrishnan, *Phys. Rev. B* **83**, 174426 (2011).
⁸K.-S. Chang, M. A. Aronova, C.-L. Lin, M. Murakami, M.-H. Yu, J. Hattrick-Simpers, O. O. Famodu, S. Y. Lee, R. Ramesh, M. Wuttig, I. Takeuchi, C. Gao, and L.A. Bendersky, *Appl. Phys. Lett.* **84**, 3091 (2004).
⁹X. Fan, D. Xue, M. Lin, Z. Zhang, D. Guo, C. Jiang, and J. Wei, *Appl. Phys. Lett.* **92**, 222505 (2008).
¹⁰H. Le Gall, J. Ben Youssef, N. Vukadinovi, and J. Ostorero, *IEEE Trans. Magn.* **38**, 2526 (2002).
¹¹Y. Lamy and B. Viala, *J. Appl. Phys.* **97**, 10F910 (2005).
¹²G. Chai, Y. Yang, J. Zhu, M. Lin, W. Sui, D. Guo, X. Li, and D. Xue, *Appl. Phys. Lett.* **96**, 012505 (2010).
¹³K. Suzuki, N. Ito, J. S. Garitaonandia, and J. D. Cashion, *J. Appl. Phys.* **99**, 08F114 (2006).
¹⁴F. Suits, *IEEE Trans. Magn.* **26**, 2353 (1990).
¹⁵V. Dubuget, A. Thiaville, F. Duverger, S. Dubourg, O. Acher, and A.-L. Adenot-Engelvin, *Phys. Rev. B* **80**, 134412 (2009).
¹⁶F. B. Hagedorn, *J. Appl. Phys.* **40**, 5179 (1969).
¹⁷K. Ishiyama, A. Toyoda, K. I. Arai, and K. Okita, *IEEE Trans. Magn.* **31**, 3841 (1995).
¹⁸S. U. Jen and W. L. Chen, *J. Appl. Phys.* **87**, 8640 (2000).
¹⁹J. F. Calleja, M. O. Gutierrez, G. Suran, J. A. Corrales, and C. Contreras, *Jpn. J. Appl. Phys.* **37**, 6384 (1998).
²⁰P. Thibaudeau, F. Ott, A. Thiaville, V. Dubuget, and F. Duverger, *Europhys. Lett.* **93**, 37003 (2011).
²¹V. Dubuget, S. Dubourg, P. Thibaudeau, and F. Duverger, *IEEE Trans. Magn.* **46**, 1139 (2010).
²²D. Pain, M. Ledieu, O. Acher, A. L. Adenot, and F. Duverger, *J. Appl. Phys.* **85**, 5151 (1999).
²³M. Ledieu, F. Schoenstein, J.-H. Le Gallou, O. Valls, S. Queste, F. Duverger, and O. Acher, *J. Appl. Phys.* **93**, 7202 (2003).
²⁴S. M. Valvidares, L. M. Alvarez-Prado, J. I. Martin, and J. M. Alameda, *Phys. Rev. B* **64**, 134423 (2001).
²⁵L. M. Alvarez-Prado and J. M. Alameda, *J. Magn. Magn. Mater.* **316**, e872 (2007).
²⁶S. Dubourg, S. Queste, and O. J. Acher, *Appl. Phys.* **97**, 10F903 (2005).
²⁷A. Yoshihara, K. Takanashi, M. Shimoda, O. Kitakami, and Y. Shimada, *Jpn. J. Appl. Phys.* **33**, 3927 (1994).
²⁸M. Rivas, J. F. Callejas, M. C. Contreras, M. Guyot, M. Porte, V. Cagan, and R. Krishnan, *J. Magn. Magn. Mater.* **148**, 129 (1995).
²⁹G. Suran, H. Ouahmane, I. Iglesias, M. Rivas, J. A. Corrales, and M. C. Contreras, *J. Appl. Phys.* **76**, 1749 (1994).
³⁰H. Hoffmann, *IEEE Trans. Magn.* **4**, 32 (1968).
³¹D. Spinato, A. Fessant, J. Gieraltowski, H. Le Gall, and C. Tannous, *J. Appl. Phys.* **85**, 6010 (1999).
³²J. F. Calleja, M. C. Contreras, M. Rivas, J. A. Corrales, G. Suran, and H. Ouahmane, *J. Magn. Magn. Mater.* **152**, 17 (1996).
³³H. J. de Wit, C. H. M. Witmer, and F. W. A. Dirne, *IEEE Trans. Magn.* **23**, 2123 (1987).
³⁴R. Krishnan, M. O. Gutiérrez, J. F. Calleja, M. C. Contreras, and A. I. Fernandez, *J. Magn. Magn. Mater.* **188**, 35 (1998).